RSC Advances

This article can be cited before page numbers have been issued, to do this please use: M. Han, Z. Gu, C. Chen, Z. Wu, Y. Que, Q. Wang, H. Wan and G. guan, *RSC Adv.*, 2016, DOI: 10.1039/C6RA00579A.

ROYAL SOCIETY OF CHEMISTRY

www.rsc.org/advances

View Article Online
DOI: 10.1039/C6RA00579A

Efficient Confinement of Ionic Liquids in the MIL-100(Fe) Frameworks by the "Impregnation-Reaction-Encapsulation" Strategy for Biodiesel Production

Mingjuan Han[a], Zheng Gu[a], Chong Chen[b], Zuowang Wu[b], Yigen Que[b], Qiang Wang[a], Hui Wan[b*], Guofeng Guan[b*]

[a] College of Chemistry and Molecular Engineering, Nanjing Tech University,

[b] College of Chemical Engineering, Nanjing Tech University, Nanjing 210009, China

[*] Corresponding author: E-mail address: wanhui@njtech.edu.cn; guangf@njtech.edu.cn

ABSTRACT:

A new, simple and effective strategy to confine dicationic acid ionic liquids (DAILs, 1,4-bis[3-(propyl-3-sulfonate) imidazolium] butane hydrogen sulfate) in the cages of MIL-100(Fe) framework was constructed. The target catalyst, defined as MIL-100(Fe)@DAILs, was characterized by XRD, FTIR, SEM, TEM, EA, TGA and N_2 adsorption-desorption. Meanwhile, the catalytic activity of MIL-100(Fe)@DAILs catalyst was evaluated by the esterification reaction with oleic acid and methanol. The results indicated that the DAILs had been effectively encapsulated within the cages of MIL-100(Fe) framework. Moreover, the influence of reaction time, reaction temperature, molar ratio of methanol to oleic acid and catalyst dosage on the conversion of oleic acid had been studied by univariate analysis. And the conversion of oleic acid decreased from 93.5% to 86.0% when the catalyst was reused five times, which indicated that the target catalyst possessed higher catalytic activity and superior catalytic activity. Finally, an esterification mechanism catalyzed by this novel catalyst was illustrated.

Keywords: Biodiesel; Ionic liquids; Metal-organic frameworks; Encapsulation

1. Introduction

Biodiesel had emerged as one of the most promising energy sources to replace current

View Article Online
DOI: 10.1039/C6RA00579A

petroleum-based diesel due to its sustainable, biodegradable and non-toxic[1, 2]. And it could be easily produced through base- or acid-catalyzed esterification and transesterification reactions[3], particularly highly reactive homogeneous Brønsted acid had been proved to be effective catalysts in esterification[4-6]. Unfortunately, homogeneous base or acid catalysts suffered from serious contamination and corrosion problems that required the implementation of good separation and purification steps, and their high costs and unendurable viscosity restricted their industrial applications[7]. Therefore, these homogeneous acid- or base-catalyzed systems were not an excellent choice for commercial application.

Recently, ionic liquids (ILs) as the new environmentally-friendly liquid acidic catalysts, had received extensive attention due to their special properties such as negligible volatility, remarkable solubility, no corrosion, non-flammable and thermal stability and especially showed the excellent catalytic activity in the synthesis of biodiesel[8, 9], but their drawbacks, such as limited solubility with organic compounds (especially polar molecules) not only caused catalysis loss but also resulted in purification difficulty, and the high viscosity of the ILs limited their industrial applications[10]. Attempts had been made to solve these problems by immobilizing acidic ILs onto silica gel[11], ordered mesoporous silica[12], polystyrene-based polymers[13] or poly divinylbenzene (PDVB)[14] and magnetic nanoparticles (MNP)[15, 16].

Meal-organic frameworks (MOFs), an emerging class of hybrid inorganic-organic porous materials, had been receiving considerable attention for their potential application in gas storage, molecular separation, heterogeneous catalysts, and catalyst

View Article Online
DOI: 10.1039/C6RA00579A

supports[17-20]. MOFs as heterogeneous catalysts or catalyst supports offered the main advantages of having the large surface area together with a large number of active sites, high porosity, regular and accessible pores, and crystalline open structures[21]. Therefore, different approaches had been employed for the introduction of strong Brønsted acidity in MOFs[22], these included mainly post-synthetic and encapsulation routes, like controlled frameworks destruction to increase the number and acidity of CUS[23], encapsulation of heteropolyacids[24], and direct synthesis of free sulfonic acid functionalized MOFs[25]. Otherwise, up to date, there were few investigations focusing on introducing the strong Brønsted acidity in MOFs matrix except for Luo and his co-workers[26] and our previous study[27]. In the above investigations, Brønsted acidic ionic liquid confined inside well-defined MIL-101 nanocages by organic electron-rich N-heterocyclic compound as a chemical bridge[26] and the anion exchange strategy[27].

Considering that iron (III) trimesate MOFs (MIL-100(Fe), MIL standing for Material of Institut Lavoisier) were effectively assembled from iron(III) trimers and trimesic acid linkers, and had two kinds of mesocages (cage diameters are 25 and 29 Å) accessible through microporous windows (5.8 and 8.6 Å)[28]. It meant iron (III) trimesate MOFs possess the regular and accessible pore size, and crystalline open structures. Therefore, if we introduced some small molecular acidic ILs to pass through the windows and stayed in the cages of MOFs, then made them react in the cages to become larger molecular acidic ILs. Efficient encapsulation could be realized when the larger ILs couldn't escape from the cages of MOFs because of their enough large bodies.

View Article Online
DOI: 10.1039/C6RA00579A

Herein, in this work, we proposed a new, simple and effective strategy to confine acid ionic liquids in porous MIL-100(Fe) frameworks. First, we chose a type of ionic liquids were easily diffused into the pores of MIL-100(Fe) frameworks, and then we attempted to excite them to grow up so that they could not escape from the cages of MIL-100(Fe) matrix. Then, the ideal MIL-100(Fe)-supported acid catalysts for their efficient catalytic activities were performed to check the validity of encapsulation by the esterification reactions. Meanwhile, the characterization of the target catalyst (defined as MIL-100(Fe)@DAILs) was studied by XRD, FTIR, SEM, TEM,EA, TGA and N_2 adsorption-desorption.

2. Experimental

2.1. Materials and instrumentation

Benzene-1,3,5-tricarboxylic acid, ferric chloride hexahydrate ($FeCl_3 \cdot 6H_2O$) were purchased from Sigma-Aldrich. Imidazole (99 %), 1,3-propane sultone (99 %), diethyl ether, methanol, ethanol, oleic acid and other chemicals were obtained from Aladdin and used without further purification.

The powder XRD experiments were done with the Smart Lab diffractometer (Rigaku, Japan) using Ni-filtered CuKα radiation (λ=0.154 nm). The materials were in advance degassed for 4 h at 150 °C, then their Nitrogen adsorption-desorption isotherms were measured using the ASAP 2020 system (Micromeritics, USA) at -196 °C. The FTIR spectra were recorded by using a Nicolet 6700 FTIR spectrometer (Thermo Fisher Scientific, USA). Scanning electron microscopy (SEM) was

View Article Online
DOI: 10.1039/C6RA00579A

performed on the S-4800 field-emission microscope (Hitachi, Japan). Transmission electron microscopy (TEM) was conducted with the JEM-2100 high-resolution transmission electron microscope (JEOL, Japan). Thermogravimetric analysis (TGA) was carried out in the temperature range of 25-600 °C (heating rate: 10 °Cmin^{-1}) under N_2 flow. Elemental analyses (EA) were conducted with Elementar Vario EL III system to determine the C, H, and N content of the prepared catalysts.

2.2. Synthesis of MIL-100(Fe)

MIL-100(Fe) was hydrothermally synthesized in the absence of HF as previously reported[24]. $FeCl_3 \cdot 6H_2O$ (2.70 g) and benzene-1,3,5-tricarboxylic acid (1.39 g) were dissolved in deionized water (50 mL). The mixture was then transferred to a Teflon-lined autoclave, and was heated at 130 °C for 72 h. The orange solid was recovered through filtration and washed several times with methanol. After the solid product had been obtained, guest molecular exchange was carried out with dichloromethane at room temperature for 3 days. Finally, the material was evacuated under vacuum at 150 °C for 12 h.

2.3. Synthesis of DAILs

AILs $[SO_3H\text{-}(CH_2)_3\text{-}HIM][HSO_4]$ were synthesized as described in our previous work[29]. DAILs $[SO_3H\text{-}(CH_2)_3\text{-}IM]_2C_4[HSO_4]_2$ were prepared as following steps. First, AILs (1.2 g) was added into methanol (20 mL) and stirred for 30 min. Second, 1,4-Dibromobutane was added dropwise at 0 °C and stirred at 25 °C for 12 h, and then the mixture was stirred at 60 °C for another 12 h. Finally, DAILs was achieved by washing with diethyl ether and drying under vacuum at 80 °C for 12 h.

View Article Online
DOI: 10.1039/C6RA00579A

2.4. Synthesis of MIL-100(Fe)@DAILs

The "impregnation-reaction-encapsulation" process of encapsulating DAILs $[SO_3H\text{-}(CH_2)_3\text{-}IM]_2C_4[HSO_4]_2$ into the framework of MIL-100(Fe) was briefly as follows. First, AILs was added into the solution of methanol(20 mL) with MIL-100(Fe)(1.0 g) and stirred for 30 min. Second, 1,4-Dibromobutane was added dropwise at 0 °C and stirred at 25 °C for 12 h, and then the mixture was stirred at 60 °C for another 12 h. Finally, the orange solid was collected through centrifugation and washed with methanol. The product was performed using hot methanol at 40 °C for 12 h and evacuated under vacuum at 80 °C for 12 h. In order to optimize the amount of DAILs species occluded in the cavities of MIL-100(Fe), the samples 1-4 with the different adding amount of AILs were shown in Table 1 and sample 2 was chosen to be the target catalyst.

MIL-100(Fe)/AILs was prepared through direct impregnation of MIL-100(Fe) with AILs. The solid was performed using hot methanol at 40 °C for 12 h and evacuated under vacuum at 80 °C for 12 h.

2.5. Catalytic reaction

The catalytic activity of MIL-100(Fe)@DAILs was evaluated by using the esterification of oleic acid with methanol. In a typical reaction, oleic acid (10 mmol) and methanol (100 mmol) were mixed in a 50 mL round bottom flask equipped with a magnetic stirrer and a water condenser system, then added an appropriate amount of the catalyst. The reaction was kept at 67 °C for 4 h. After the reaction, the catalyst was separated from the reaction mixture by centrifugation, washed with copious amounts

View Article Online
DOI: 10.1039/C6RA00579A

of methanol, performed using hot methanol at 40 °C for 12 h and evacuated under vacuum at 80 °C for 12 h. A gas chromatograph equipped with a flame ionization detector (SP-6890; SE-54 capillary column: 30 m×0.25 mm×0.3 mm) was employed to analyze the conversion of oleic acid.

3. Results and discussion

3.1. Characterization of the catalysts

The XRD patterns of MIL-100(Fe), MIL-100(Fe)@DAILs and the recovered MIL-100(Fe)@DAILs in Fig. 1 showed that the diffraction peaks of MIL-100(Fe) were consistent with its standard XRD data reported in the literature[30]. The slight decrease in relative intensities could be found at 2-5°, which indicated that the encapsulation of ILs in MIL-100(Fe) matrix had changed its crystal structure[24]. Compared with MIL-100(Fe)@DAILs (Fig. 1b), the diffraction peaks of recovered MIL-100(Fe)@DAILs(Fig. 1c) were almost unchanged. The result showed that the crystal structure of target catalyst was stable after the catalytic reaction.

As shown in Fig. 2, the FTIR spectra of AILs, DAILs, MIL-100(Fe) and MIL-100(Fe)@DAILs were recorded in the spectral range 400-4000 cm^{-1}. The peak of DAIL at 3443 cm^{-1} was related to O-H vibrations of physical adsorbed water in Fig. 2b, and the peak of AILs at this area was related to ν(N－H) stretching vibration Fig. 2a. The characteristic peaks of MIL-100(Fe) at 1714, 1382, and 1600-1446 cm^{-1} could be observed in Figs. 2c, 2d and 2e. The peaks were attributed to ν(C=O)stretching vibration, ν(C－O) stretching vibration and ν(C=C) vibrations of aromatic groups in

View Article Online
DOI: 10.1039/C6RA00579A

MIL-100(Fe) matrix, respectively. The peaks (at 1580, 1217, 1035 and 3443 cm^{-1} in Fig. 2b) of DAILs were also displayed in Figs. 2d and 2e, which were related to ν(C=N) stretching vibrations in imidazole ring, ν(S=O) asymmetric, symmetric stretching vibrations of sulfonic acid group and O-H vibrations of physical adsorbed water, respectively. This indicated DAILs were successfully encapsulated in MIL-100(Fe) matrix. To further confirm above discussion, the optimized geometric structures of the AILs, DAILs and Oleic acid were optimized by a semi-empirical PM3 method and using Gaussian09 program package (revision B.01; Gaussian, Inc., Wallingford CT, 2010), as shown in Fig. 3. First, AILs (L: 1.05 nm; W: 0.6 nm, shown in Figs. 3a) could pass through the bigger hexagonal windows (~0.86 nm, shown in Figs. 3d) of big mesoporous cages, therefore, AILs easily diffused into the microcages of MOFs. Then, according to the optimized geometric structures of DAILs (L: 1.93 nm; W: 0.9 nm, shown in Fig. 3b), an efficient encapsulation could be realized since the MIL-100(Fe) had the big mesocages with diameters of 2.9 nm and accessible microporous windows of 0.86 nm. It indicated that DAILs could stay in the big mesocages and could not escape from the windows of 0.86 nm due to their enough large bodies. Finally, the results showed that the optimized geometric structures of the oleic acid were close to 2.35 nm (length) and 0.35 nm (width) (shown in Fig.3c), and it indicated that the carboxyl terminal of oleic acid molecules could smoothly insert through the windows of 0.6 nm or 0.86 nm and react with active components. In conclusion, both FTIR spectra and semi-empirical PM3 method proved DAILs were successfully confined in the frameworks of MIL-100(Fe) by the

View Article Online
DOI: 10.1039/C6RA00579A

"impregnation-reaction-encapsulation" strategy.

The MIL-100(Fe) kept the same well-defined octahedral shape before and after the encapsulation of DAILs, as investigated by SEM and TEM (Fig. 4). The average particles size of MIL-100(Fe) and MIL-100(Fe)@DAILs was about 500 nm, only the external surface of MIL-100(Fe)@DAILs tended to become rough. In comparison to the pristine MIL-100(Fe), the crystal morphology of the recovered catalyst had changed slightly and the average particles size was still approximately 500 nm, which suggested that catalytic reaction would have little effect on the carrier structure.

In order to further investigate the target catalysts, the N_2 adsorption-desorption isotherms of MIL-100(Fe) and MIL-100(Fe)@DAILs were exhibited in Fig. 5. As same as the pristine MIL-100(Fe), the N_2 isotherm of MIL-100(Fe)@DAILs exhibited a type-I/IV mixed type isotherm. The surface area and total pore volume decreased from 1183.7 to 170.2 m^2g^{-1} and from 0.72 to 0.20 cm^3g^{-1} for MIL-100(Fe) and MIL-100(Fe)@DAILs, respectively. The decreasing BET surface area and pore volume could be attributed to the presence of DAILs inside the MIL-100(Fe) nanocages. Moreover, the open cavities and high surface areas were retained, which benefited the free diffusion of the reactants or products. The elemental analysis (C 26.25, H 3.24, N 4.97) of MIL-100(Fe)@DAILs showed that DAILs were effectively encapsulated into MIL-100(Fe), and the loading amount was 0.8875 $mmolg^{-1}$ by the calculation of the nitrogen content. In conclusion, all results confirmed the effective encapsulation of DAILs within the cages of MIL-100(Fe).

TGA curves of MIL-100(Fe) and MIL-100(Fe)@DAILs were shown in Fig. 6. At the

View Article Online
DOI: 10.1039/C6RA00579A

temperature below 250 °C, the weight loss of MIL-100(Fe) (almost 30%) and MIL-100(Fe)@DAILs (<10%) were resulted from the adsorbed water on the inner and outer surfaces of the frameworks of MIL-100(Fe). Due to the occupation of DAILs inside the MOFs pore, MIL-100(Fe)@DAILs showed less weight loss than the pristine MIL-100(Fe). There was a rapid weight loss of MIL-100(Fe)@DAILs in the temperature range of 250-350 °C, which was attributed to decomposition of DAILs. When the temperature increased above 350 °C, MIL-100(Fe) begun to degrade with the decomposition of benzene-1,3,5-tricarboxylic acid and the collapse of the MIL-100(Fe) framework.

3.2. Catalytic activity

3.2.1. Conversion of oleic acid catalyzed by samples 1-4

In order to optimize the amount of DAILs species occluded in the cavities of MIL-100(Fe), the loading amount, surface area, total pore volume and conversion of the samples were characterized and shown in Table 1. Table 1 showed that the loading amount calculated by the elemental analysis was increased from 0.6786 to 0.9678 $mmolg^{-1}$ when the AILs were added from 0.8 g to 2.0 g, correspondingly, the surface area and total pore volume decreased from 232.1 to 118.0 m^2g^{-1} and from 0.26 to 0.17 cm^3g^{-1}, respectively. Meanwhile, the conversion of oleic acid was increased to the maximum value (conversion: 89.5%), then decreased to 87.8% when the AILs were continuously added. The main reason for this was because the cavities of MIL-100(Fe) were occluded by the more DAILs and couldn't give enough room to facilitate the access of oleic acid molecules.

View Article Online
DOI: 10.1039/C6RA00579A

3.2.2. Univariate analysis

The catalytic activity of MIL-100(Fe)@DAILs was evaluated by the esterification reaction with oleic acid and methanol. Univariate analysis[15] was conducted to study the influence of reaction time, reaction temperature, molar ratio of methanol to oleic acid and catalyst dosage on the conversion of biodiesel, as shown in Fig. 7.

Fig. 7a showed that the conversion of oleic acid was first increased and then slightly decreased with increasing the reaction time, the maximum value was 92.6% when the time was 5 h. At the beginning of the reaction, the catalyst could not contact with reactants adequately, so the conversion rate was not high, but as the time increased, the conversion rate of oleic acid increased due to enough contact. The effect of temperature on the conversion of oleic acid was shown in Fig. 7b. It showed that the conversion of oleic acid was increased with the increment of reaction temperature (up to 67 °C), and then slightly decreased, which was attributed to the change of catalytic activity of MIL-100(Fe)@DAILs with temperature. Considering both energy conservation and environmental protection, the most suitable reaction temperature was 67 °C. In Fig. 7c, it was observed that the conversion of oleic acid increased with increasing the molar ratio of methanol to oleic acid (up to 8:1) and then kept constant, when reaction time and temperature were kept at 5 h and 67 °C, respectively. The reasons for this were: more dosage of methanol benefited to the dispersion of the MIL-100(Fe)@DAILs catalyst and increased the chance of collision between reactants and catalyst from the molecular level. The influence of catalyst dosage on the conversion of oleic acid was studied at 5 h, 67 °C and molar ratio of methanol to

View Article Online
DOI: 10.1039/C6RA00579A

oleic acid 8:1, as displayed in Fig. 7d. When adding more catalysts, the conversion of oleic acid was higher because of the adequate number of active sites.

Based on the above analysis, the optimized experimental conditions were obtained: reaction time 5 h, reaction temperature 67 °C, molar ratio of methanol to oleic acid 8:1 and catalyst dosage 15 wt%, and then the conversion of oleic acid reached 93.5%.

3.3. Catalytic activities of different catalysts

To test the catalytic activity of target catalyst (MIL-100(Fe)@DAILs), the catalytic activities of different catalysts (some from references[31-34] and some from our work) for the esterification of oleic acid were compared with each other and shown in Table 2. It should be noted that reaction conditions performed by us were reaction time 5 h, reaction temperature 67 °C, molar ratio of methanol to oleic acid 8:1 and catalyst dosage 15 wt%. As shown in Table 2, first, the esterification reaction seemed to hardly perform without a catalyst (entry 1). Second, entries 2-3 showed that homogeneous catalysts (AILs and DAILs) possessed high catalytic activities due to their typical properties of Brønsted acid. Third, the pristine MIL-100(Fe) also showed catalytic performance (shown in entry 4) due to the Lewis acid sites which provided by the unsaturated coordinated metal centers (Fe^{III}). Fourth, the excellent catalytic activities from heterogeneous catalysts (MIL-100(Fe)/AILs and MIL-100(Fe) @DAILs) could be obtained because of the typical property of Brønsted acid from ILs, and the Lewis acid sites from the pristine MIL-100(Fe)). The heterogeneous catalysts were our target catalysts due to their easy separation although the catalytic activities of homogeneous ionic liquids were high. Finally, in order to further prove the excellent catalytic

View Article Online
DOI: 10.1039/C6RA00579A

activities of target catalysts, we employed some catalysts from references (entries 7-10) to compare with our target catalysts. All the results showed that the target catalysts MIL-100(Fe)/AILs and MIL-100(Fe)@DAILs could be the promising and excellent catalysts for esterification reaction.

3. 3. Reusability of the catalyst

It was necessary to test the reusability of catalysts, therefore, the esterification reactions catalyzed by heterogeneous catalysts (MIL-100(Fe)/AILs and MIL-100(Fe) @DAILs) were carried out for six times under the optimized experimental condition, shown in Fig. 8. After each reaction, the catalysts were recovered by centrifugation, dried under vacuum and reused in the subsequent reaction. From Fig. 8, it showed that the conversion of oleic acid decreased from 93.5% to 86.0% for MIL-100(Fe)@DAILs catalyst, otherwise, sharply decreased from 90.2% to 22.3% for MIL-100(Fe)/AILs catalyst, when the catalyst was reused five times. Therefore, this result indicated the MIL-100(Fe)@DAILs catalyst possessed the higher reusability than that of MIL-100(Fe)/AILs catalyst and could be used in industry. The slight decrease of conversion for MIL-100(Fe)@DAILs catalyst might be due to mass loss of blockage of MOFs channels and it was natural phenomenon. It was obvious that conversion of MIL-100(Fe)/AILs were sharply decreased from 90.2% to 22.3%, which could be attributed to major leaching of ILs from the channels of MOFs. All in all, the results confirmed that the DAILs were effectively encapsulated into the MOF cages, and the target catalyst MIL-100(Fe)@DAILs possessed superior catalytic activity.

View Article Online
DOI: 10.1039/C6RA00579A

3. 4. Mechanism of esterification

The classical esterification mechanism had two key steps, one was the protonation of oleic acid and the other was the nucleophilic attack of the protonated acid by the short-chain alcohol[11]. Therefore, the esterification mechanism of oleic acid catalyzed by the target catalyst MIL-100(Fe)@DAILs could be displayed in Fig.9 and the whole process was divided into five steps. First, DAILs encapsulated within the framework of MIL-100(Fe) would support the proton, and oleic acid was protonated to generate a carbocation (product 2). Second, the nucleophilic attack of the methanol molecule to the carbocation generated a middle product (product 3). Third, the protonated hydroxyl in product 4 had been formed when H^+ of product 3 transferred. Fourth, one molecule water took off the backbone of product 4. Finally, methyl oleate and catalyst were recovered when the bond of hydrogen and oxygen of product 5 had been broken.

4. Conclusion

DAILs were effectively encapsulated within the framework of MIL-100(Fe) by an "impregnation-reaction-encapsulation" strategy, and confirmed by corresponding techniques. The catalytic activity of MIL-100(Fe)@DAILs was evaluated by the esterification reaction with oleic acid and methanol. The optimized experimental condition was obtained: reaction time 5 h, reaction temperature 67 °C, molar ratio of methanol to oleic acid 8:1 and catalyst dosage 15 wt%, and then the highest conversion of oleic acid reached 93.5%. Moreover, the conversion of oleic acid decreased from 93.5% to 86.0% when the catalyst was reused six times. The results

View Article Online
DOI: 10.1039/C6RA00579A

showed that the catalyst possessed superior catalytic activity and could be easily recovered without obvious leaching of the active component.

Acknowledgments

We gratefully acknowledge the National Natural Science Foundation of China (21476110, 21003074, 21176121 and 21373112), the Key Project for University Natural Science Foundation of Jiangsu Province (14KJA530001) and the Natural Science Foundation of Jiangsu Province (BK20131407, BK20151531), the Foundation from State Key Laboratory of Materials-oriented Chemical Engineering, Nanjing Tech University(ZK201305), the Research Innovation Training Project for Graduate Students of Jiangsu Province(KYZZ_0227), and the Practice and Innovation Training Project for College Students of Jiangsu Province(201410291041Z, 201310291036Z) for financial support.

References

1. A. Demirbas, *Energ. Convers. Manage.*, 2009, **50**, 14-34.
2. M. E. Borges and L. Díaz, *Renew. Sust. Energ. Rev.*, 2012, **16**, 2839-2849.
3. F. Su and Y. Guo, *Green. Chem.*, 2014, **16**, 2934-2957.
4. D.-W. Lee and K.-Y. Lee, *Catal. Surv. Asia.*, 2014, **18**, 55-74.
5. Y. Zang, J. Shi, F. Zhang, Y. Zhong and W. Zhu, *Catal. Sci. Technol.*, 2013, **3**, 2044.
6. F. Zhang, Y. Jin, J. Shi, Y. Zhong, W. Zhu and M. S. El-Shall, *Chem. Eng. J.*, 2015, **269**, 236-244.
7. C. P. Mehnert, R. A. Cook, N. C. Dispenziere and M. Afeworki, *J. Am. Chem. Soc.*, 2002, **124**.
8. Q. Wu, H. Chen, M. Han, D. Wang and J. Wang, *Ind. Eng. Chem. Res.*, 2007, **46**, 7955-7960.
9. M. Ghiaci, B. Aghabarari, S. Habibollahi and A. Gil, *Bioresource. Technol.*, 2011, **102**, 1200-1204.
10. H. Li, P. S. Bhadury, B. Song and S. Yang, *RSC Adv.*, 2012, **2**, 12525.
11. J. Miao, H. Wan, Y. Shao, G. Guan and B. Xu, *J. Mol. Catal. A-Chem.*, 2011, **348**, 77-82.
12. B. Karimi and M. Vafaeezadeh, *Chem. Commun.*, 2012, **48**, 3327-3329.
13. Z. Xu, H. Wan, J. Miao, M. Han, C. Yang and G. Guan, *J. Mol. Catal. A-Chem.*, 2010, **332**,

View Article Online
DOI: 10.1039/C6RA00579A

152-157.
14. X. Liang, *Ind. Eng. Chem. Res.*, 2013, **52**, 6894-6900.
15. H. Wan, Z. Wu, W. Chen, G. Guan, Y. Cai, C. Chen, Z. Li and X. Liu, *J. Mol. Catal. A-Chem.*, 2015, **398**, 127-132.
16. Q. Zhang, H. Su, J. Luo and Y. Wei, *Green. Chem.*, 2012, **14**, 201-208.
17. A. U. Czaja, N. Trukhan and U. Muller, *Chem. Soc. Rev.*, 2009, **38**, 1284-1293.
18. A. Dhakshinamoorthy, M. Alvaro and H. Garcia, *Chem. Commun.* , 2012, **48**, 11275-11288.
19. Y. Jin, J. Shi, F. Zhang, Y. Zhong and W. Zhu, *J. Mol. Catal. A-Chem.*, 2014, **383-384**, 167-171.
20. F. Zhang, J. Shi, Y. Jin, Y. Fu, Y. Zhong and W. Zhu, *Chem. Eng. J.*, 2015, **259**, 183-190.
21. F. Vermoortele, M. Vandichel, B. Van de Voorde, R. Ameloot, M. Waroquier, V. Van Speybroeck and D. E. De Vos, *Angew. Chem. Int. Ed.*, 2012, **51**, 4887-4890.
22. J. Juan-Alcañiz, R. Gielisse, A. B. Lago, E. V. Ramos-Fernandez, P. Serra-Crespo, T. Devic, N. Guillou, C. Serre, F. Kapteijn and J. Gascon, *Catal. Sci. Technol.*, 2013, **3**, 2311.
23. F. Vermoortele, R. Ameloot, L. Alaerts, R. Matthessen, B. Carlier, E. V. R. Fernandez, J. Gascon, F. Kapteijn and D. E. De Vos, *J. Mater. Chem.*, 2012, **22**, 10313.
24. R. Canioni, C. Roch-Marchal, F. Sécheresse, P. Horcajada, C. Serre, M. Hardi-Dan, G. Férey, J.-M. Grenèche, F. Lefebvre, J.-S. Chang, Y.-K. Hwang, O. Lebedev, S. Turner and G. Van Tendeloo, *J. Mater. Chem.*, 2011, **21**, 1226-1233.
25. M. Lin Foo, S. Horike, T. Fukushima, Y. Hijikata, Y. Kubota, M. Takata and S. Kitagawa, *Dalton. T.*, 2012, **41**, 13791-13794.
26. Q.-x. Luo, M. Ji, M.-h. Lu, C. Hao, J.-s. Qiu and Y.-q. Li, *J. Mater. Chem. A.*, 2013, **1**, 6530.
27. H. Wan, C. Chen, Z. Wu, Y. Que, Y. Feng, W. Wang, L. Wang, G. Guan and X. Liu, *ChemCatChem*, 2015, **7**, 441-449.
28. V. Agostoni, T. Chalati, P. Horcajada, H. Willaime, R. Anand, N. Semiramoth, T. Baati, S. Hall, G. Maurin, H. Chacun, K. Bouchemal, C. Martineau, F. Taulelle, P. Couvreur, C. Rogez-Kreuz, P. Clayette, S. Monti, C. Serre and R. Gref, *Adv. Healthc. Mater.*, 2013, **2**, 1630-1637.
29. Z. Wu, Z. Li, G. Wu, L. Wang, S. Lu, L. Wang, H. Wan and G. Guan, *Ind. Eng. Chem. Res.*, 2014, **53**, 3040-3046.
30. P. Horcajada, S. Surble, C. Serre, D. Y. Hong, Y. K. Seo, J. S. Chang, J. M. Greneche, I. Margiolaki and G. Ferey, *Chem. Commun.*, 2007, **27**, 2820-2822.
31. Y. Jiang, J. Lu, K. Sun, L. Ma and J. Ding, *Energ. Convers. Manage.*, 2013, **76**, 980-985.
32. A. H. Mohammad Fauzi, N. A. S. Amin and R. Mat, *Appl. Energ.*, 2014, **114**, 809-818.
33. A. H. Mohammad Fauzi and N. A. Saidina Amin, *Energ. Convers. Manage.*, 2013, **76**, 818-827.
34. Q. Wu, H. Wan, H. Li, H. Song and T. Chu, *Cataly. Today.*, 2013, **200**, 74-79.

View Article Online
DOI: 10.1039/C6RA00579A

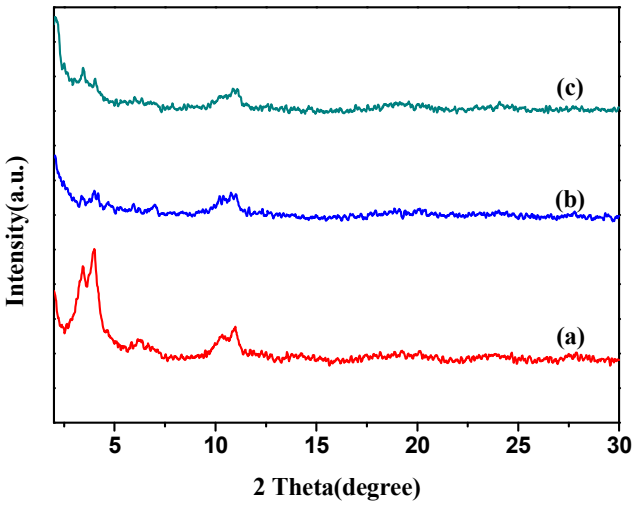

Fig.1. XRD patterns of (a) MIL-100(Fe), (b) MIL-100(Fe)@DAILs, and (c) recovered MIL-100(Fe)@DAILs.

View Article Online
DOI: 10.1039/C6RA00579A

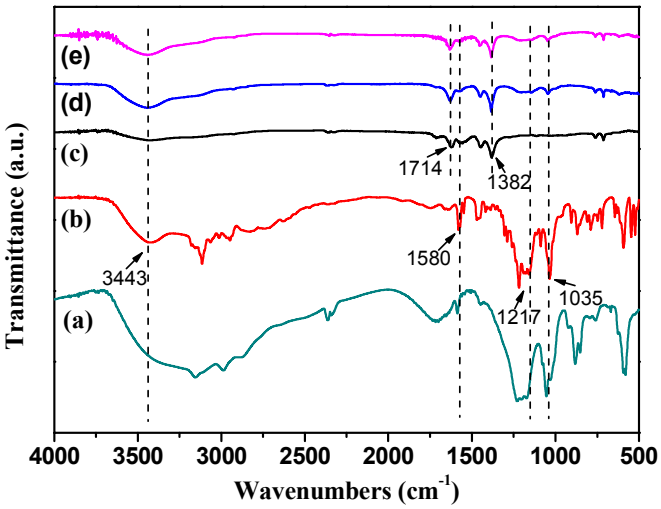

Fig. 2. FTIR spectra of (a) AILs, (b) DAILs, (c) MIL-100(Fe), (d)MIL-100(Fe)@DAILs and (e) recovered MIL-100(Fe)@DAILs.

View Article Online
DOI: 10.1039/C6RA00579A

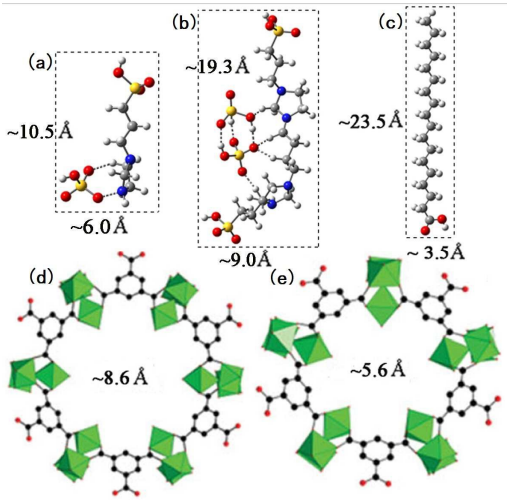

Fig 3. Optimized geometric structures of the AILs (a), DAILs (b) and oleic acid (c) were fully optimized by a semi-empirical PM3 method and using Gaussian09 program package (revision B.01; Gaussian, Inc., Wallingford CT, 2010.); Note: bigger hexagonal windows (d) for the MIL-100(Fe) was deduced from previous report[28], big mesoporous cages and smaller pentagonal opening (e)of small mesoporous cages.

View Article Online
DOI: 10.1039/C6RA00579A

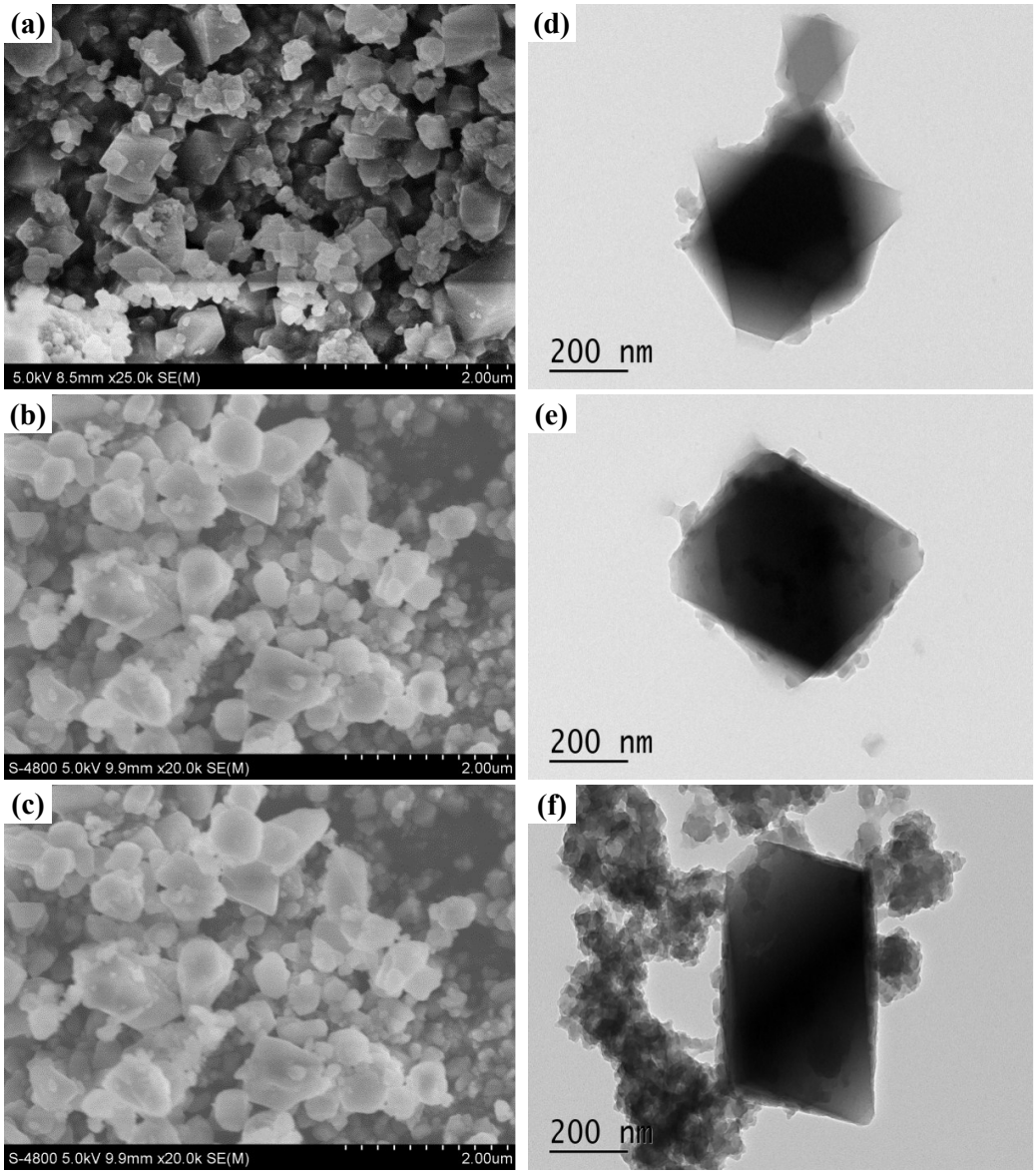

Fig. 4. SEM images (a, b, c) and TEM images (d, e, f): MIL-100(Fe)(a, d); MIL-100(Fe)@DAILs(b, e); recovered MIL-100(Fe)@DAILs(c, f).

View Article Online
DOI: 10.1039/C6RA00579A

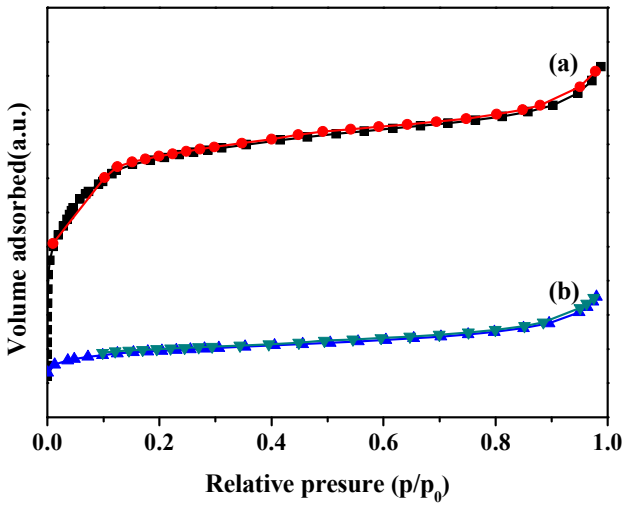

Fig. 5. N_2 adsorption-desorption isotherms of (a) MIL-100(Fe) and (b) MIL-100(Fe)@DAILs.

View Article Online
DOI: 10.1039/C6RA00579A

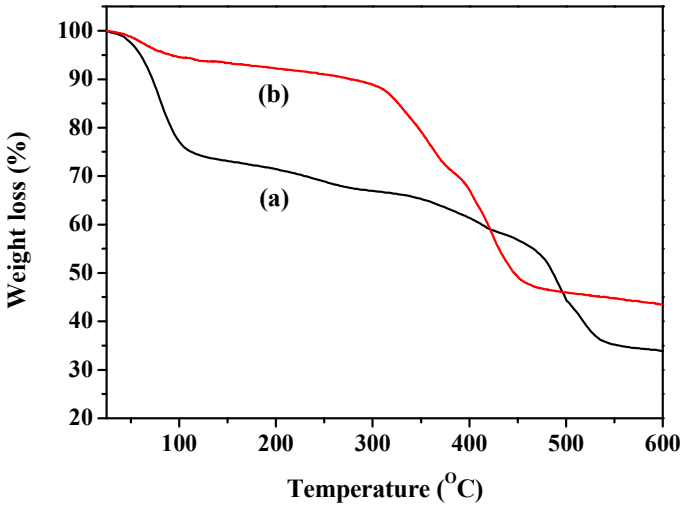

Fig. 6. TGA curves of (a) MIL-100(Fe) and (b) MIL-100(Fe)@DAILs.

View Article Online
DOI: 10.1039/C6RA00579A

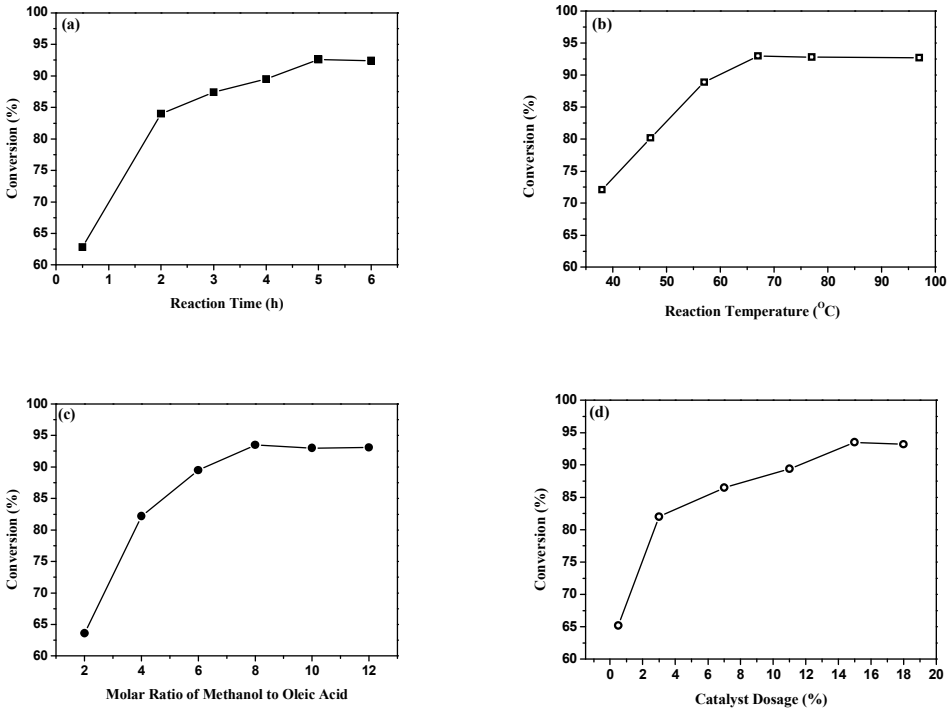

Fig. 7. Optimization of esterification of oleic acid catalyzed by MIL-100(Fe)@DAILs: reaction time (a), (77 °C, 10:1, 15 wt%); reaction temperature (b), (5 h, 10:1, 15 wt%); methanol/oleic acid molar ratio (c), (5 h, 67 °C, 15 wt%); catalyst dosage (d), (5 h, 67 °C, 8:1).

View Article Online
DOI: 10.1039/C6RA00579A

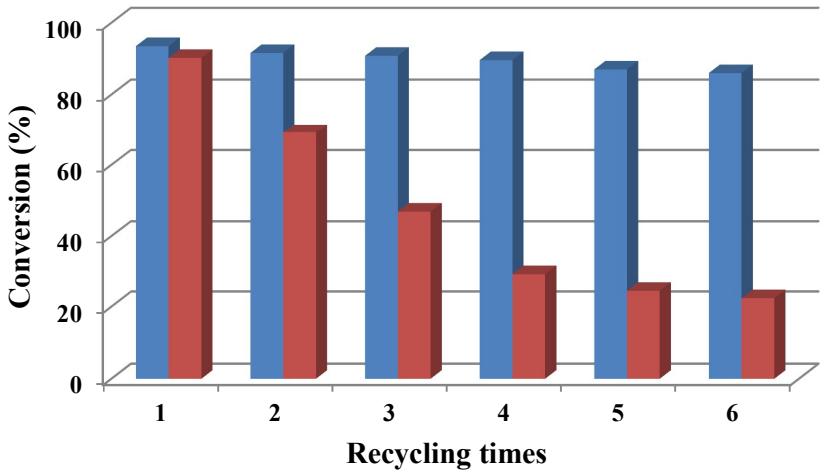

Fig. 8. Recycling of MIL-100(Fe)@DAILs (blue) and MIL-100(Fe)/AILs (red) for the esterification of oleic acid with methanol under the experimental conditions.

View Article Online
DOI: 10.1039/C6RA00579A

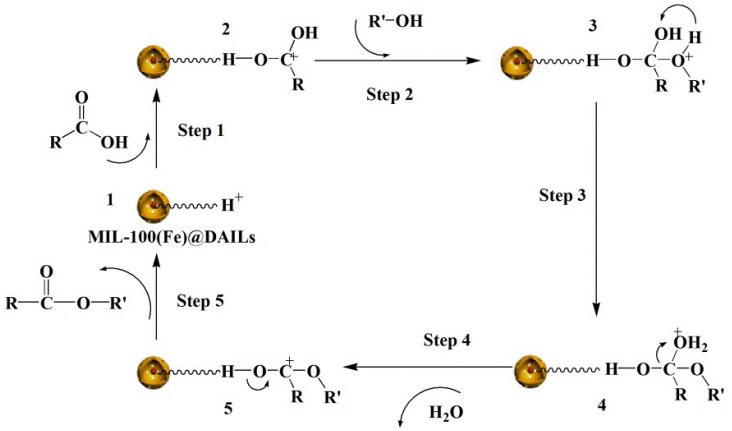

Fig. 9. Mechanism of esterification catalyzed by MIL-100(Fe)@DAILs, R=$CH_3(CH_2)_7CH=CH(CH_2)_7$, R'=$CH_3$.

View Article Online
DOI: 10.1039/C6RA00579A

Table 1. The loading amount, surface area, total pore volume and conversion of oleic acid with the different samples.

Sample	$m_{MIL-100(Fe)}$ /g	m_{AILs} /g	Loading amount /mmolg^{-1}	Surface area /m^2g^{-1}	Total pore volume /cm^3g^{-1}	Conversion /%
1	1.0 g	0.8 g	0.6786	232.1	0.26	83.6
2	1.0 g	1.2 g	0.8875	170.2	0.20	89.5
3	1.0 g	1.6 g	0.9250	146.4	0.19	88.2
4	1.0 g	2.0 g	0.9678	118.0	0.17	87.8

View Article Online
DOI: 10.1039/C6RA00579A

Table 2. Catalytic activities of different catalysts for the esterification of oleic acid.

Entry	Catalyst	Alcohol	Alcohol/Acid	Conversion/%	Reference
1	Without catalyst	methanol	8:1	4.4	This work
2	AILs	methanol	8:1	94.5	This work
3	DAILs	methanol	8:1	94.2	This work
4	MIL-100(Fe)	methanol	8:1	12.8	This work
5	MIL-100(Fe)/AILs	methanol	8:1	90.2	This work
6	MIL-100(Fe)@DAILs	methanol	8:1	93.5	This work
7	Exchange resin	ethanol	9:1	93.0	31
8	[BMIM][$FeCl_4$][a]	methanol	22:1	83.4	32
9	[BMIM][HSO_4]	methanol	9:1	80.6	33
10	MPEG-350-ILs[b]	methanol	10:1	84.5	34

[a] BMIM=1-Butyl-3-methylimidazolium,

[b] MPEG-350=Polyethylene glycol monomethylether (polymerization degree=350); ILs=[SO_3H-$(CH_2)_4$-HIM][HSO_4].

View Article Online
DOI: 10.1039/C6RA00579A

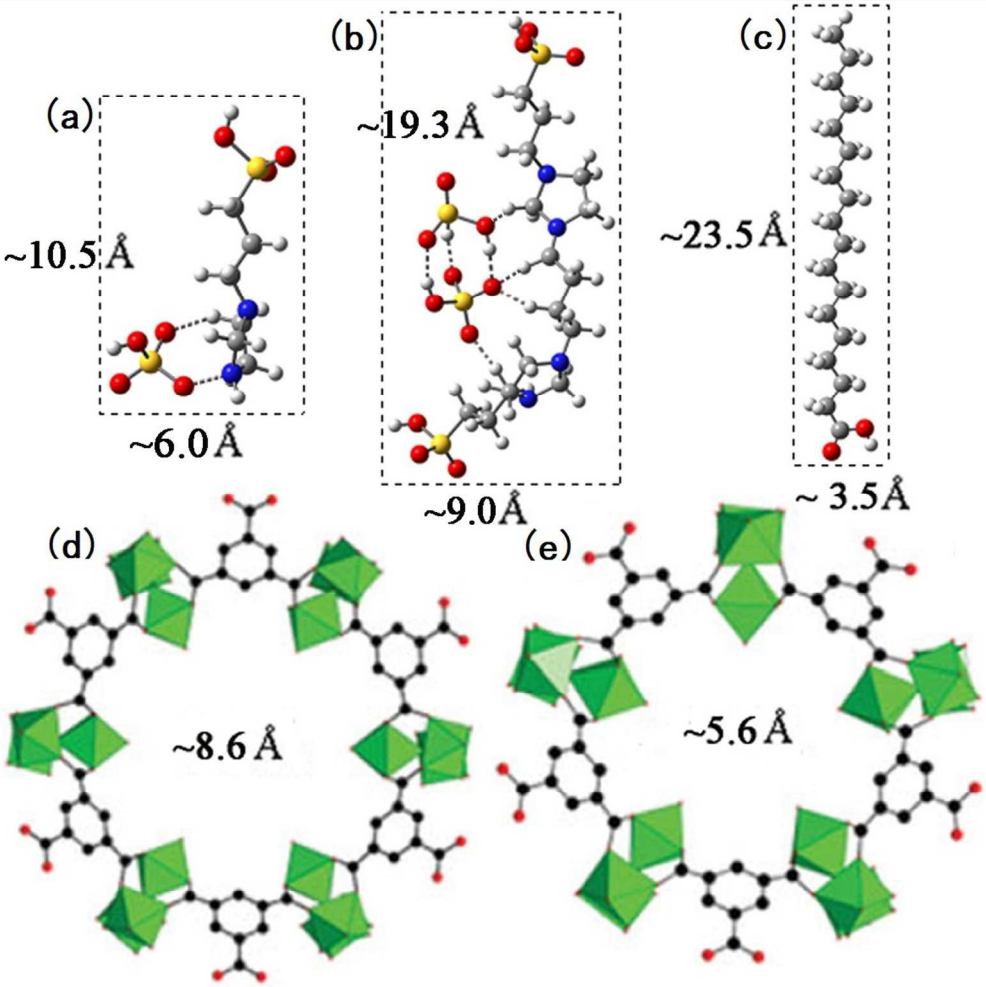

99x98mm (300 x 300 DPI)